Quaternary International 462 (2017) 75–89

Contents lists available at ScienceDirect

Quaternary International

journal homepage: www.elsevier.com/locate/quaint

Holocene shortening rates and seismic hazard assessment for the frontal Potwar Plateau, NW Himalaya of Pakistan: Insights from ^{10}Be concentrations on fluvial terraces of the Mahesian Anticline

J. Cortés-Aranda [a, b, *], J.-L. Mugnier [a], F. Jouanne [a], R. Vassallo [a, c], J. Carcaillet [d, e], A. Alam Awan [f]

[a] ISTerre Chambéry, France
[b] Departamento de Ciencias de la Tierra, Universidad de Concepción, Chile
[c] Université Savoie Mont Blanc, CNRS, 73376 Bourget du Lac, France
[d] ISTerre Grenoble, France
[e] Université Grenoble Alpes, 38400 Saint-Martin-d'Hères, France
[f] Geological Survey of Pakistan, Pakistan

ARTICLE INFO

Article history:
Received 18 March 2016
Received in revised form
7 February 2017
Accepted 27 February 2017
Available online 8 March 2017

ABSTRACT

We present the results of a structural neotectonic survey undertaken on the Mahesian Anticline in the frontal Himalaya of Pakistan. This anticline resulted from the folding of Precambrian to Tertiary layers that was controlled by a thrust and a backthrust, interacting in a complex way. Four generations of fluvial terraces formed by the Jhelum River and two tributaries have been distinguished on the SE flank of the anticline. Two of these terraces, T2 and T3, have been left hanging by fold development and have been dated by cosmogenic ^{10}Be to 6.5 ± 0.2 ka and 3.3 ± 0.7 ka, respectively. From such ages an uplift rate of ~10 mm/y was determined for the Holocene. That uplift is induced by a shortening rate of ~10 mm/y. We highlight that the Mahesian Anticline and Frontal Salt Range Thrust, together with the Kalabagh western lateral ramp and the Jhelum eastern lateral ramp, delineate the active tectonic boundary of the Potwar Plateau. This thrust sheet moves above the salt level without out-of-sequence deformation. Moreover, the small but significant difference between the long-term deformation rates (8.4 mm/y) and the geodetic velocities (2–5 mm/y) detected for the Central Potwar Plateau seems to be linked to episodic spurts of accelerated creeping of the thick salt level, triggered by earthquakes located to the north on the deep (>15 km) part of the MHT. In addition, the large difference between the long-term deformation rates and the geodetic velocities (less than 2 mm/y) reported for the eastern Potwar Plateau seems to be linked to the accumulation of a slip deficit around asperities formed where the salt is missing. This deficit may be recovered during earthquakes potentially as great as Mw 7.

1. Introduction

The Himalaya of Pakistan is characterized by regional-scale plateaus that mainly slip aseismically over the Indian Plate, as suggested from the lack of historical high-magnitude earthquakes in the area (e.g. Seeber and Armbruster, 1981, Fig. 1a and b). The largest of these plateaus is the Potwar Plateau, which bounds the western flank of the Hazara-Kashmir Syntax (e.g. Grelaud et al., 2002, Fig. 1a and b). This plateau is currently moving southwards above a late Precambrian–Early Cambrian salt level (Crawford, 1974) that partially defines the main detachment in the area: The Main Himalayan Thrust (MHT) (Schelling and Arita, 1991). It is indeed this salt unit which mostly precludes the generation of earthquakes in the area, unlike what occurs in most of the Himalaya frontal zones (e.g. Seeber and Armbruster, 1981). By combining paleomagnetic data and geological observations, Jaumé and Lillie (1988) propose that the northern Potwar Plateau deformed as a steeply tapered thrust wedge (*sensu* Chapple (1978), with an angle of 3.5°–5.5°, until ca. 2 Ma. Between 2 Ma and the Present, the propagating to the south main detachment reached the evaporates level, which has pushed the Potwar Plateau without frictional deformation. Then, erosion has reduced the initial steep slope of the plateau to its present gentle slope. Cotton and Koyi (2000),

* Corresponding author. Current address: Departamento de Ciencias de la Tierra, Universidad de Concepción, Chile.
E-mail address: joacortes@udec.cl (J. Cortés-Aranda).

http://dx.doi.org/10.1016/j.quaint.2017.02.032
1040-6182/

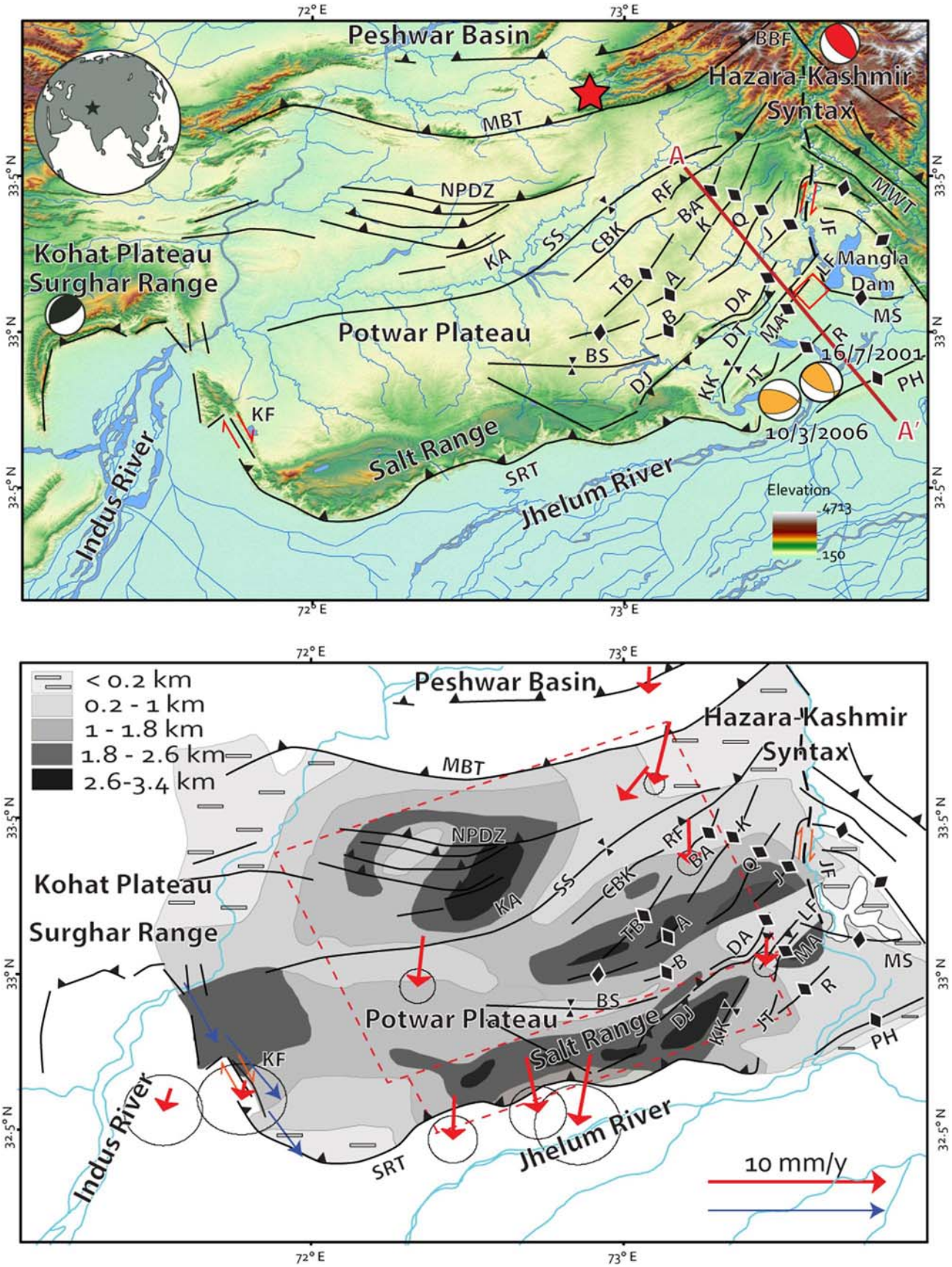

Fig. 1. a) Structural map of the Potwar Plateau-Salt Range area. The study area is delimited by a red rectangle. AA′ is the profile shown in Fig. 2b. Moment tensor solutions are provided for the 1992 Kohat Plateau and 2005 Kashmir earthquakes (black and red, respectively). Other constrained moment tensor solutions compiled are depicted by orange focal mechanisms. The approximate location of the AD 25 Taxila Earthquake is depicted by a red star, b) Isopach map of the salt detachment according to Leathers (1987). Thickness are

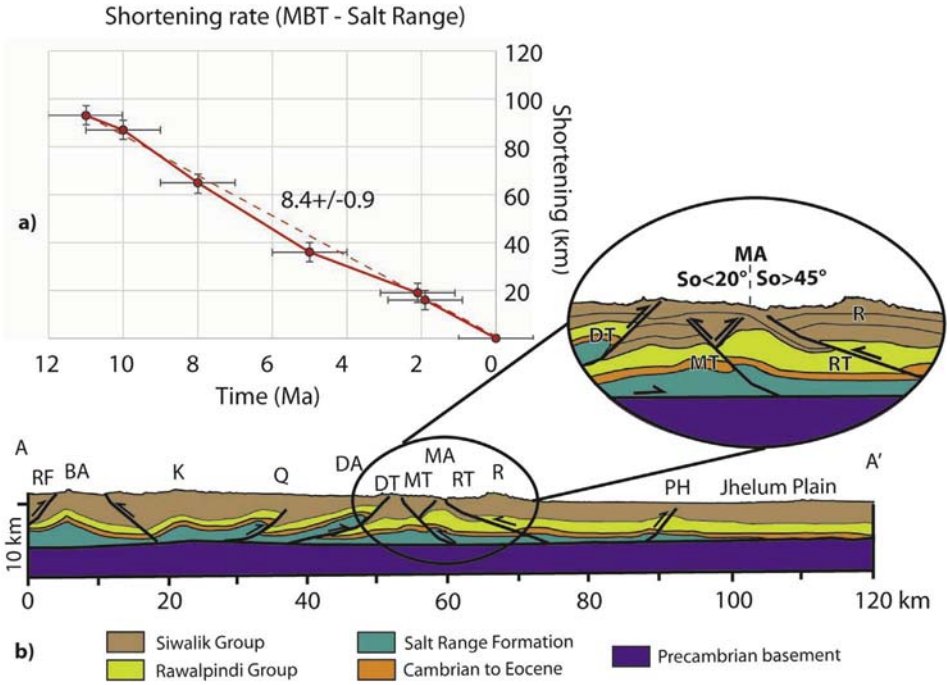

Fig. 2. a) Long term shortening rate for the MBT-Salt Range area. The mean shortening rate (dashed line) has been 8.4 ± 0.5 mm/yr since ~12 Ma. See references in text and Table Ai-ii in supplementary materials. b) Schematic profile AA′ (NW–SE) for the Potwar Plateau-Salt Range based on Leathers (1987). For location see Fig. 1a. PH = Pabbi-Hills Anticline, R = Rhodas Anticline, RT = Rhodas Thrust; MA = Mahesian Anticline, MT = Mahesian Thrust; DA = Domeli Anticline, DT = Domeli Thrust; Q = Qazian Anticline, K = Kallar Anticline; BA = Buttar Anticline, RF = Riwat Fault, SS = Soan Syncline. The ellipse is a zoom showing the change in dip of the Siwalik from the western to the eastern part of the Mahesian Anticline.

based on scaled sandbox models, simulate the evolution of the Potwar Plateau and surrounding areas above adjacent frictional and ductile substrates. Considering variations in the original thickness of the ductile salt level and the influence of the prekinematic and synkinematic style of the wedge above the main detachment, they establish that forward-vergent thrusts producing steep wedges develop above a frictional substrate. On the other hand, they suggest that both forward and backward vergent thrusts conducting low taper wedges occur over ductile substrates. Further, above a ductile level, deformation propagates farther and faster than above a frictional level; this differential rates produce a lateral inflection zone sub-parallel to the shortening direction. Within the wedge above the salt horizon, a frontal inflection and general folding is promoted, generating diapiric structures. These features are like those dominating the Salt Range - Potwar Plateau (e.g. Leathers, 1987).

Geodetic velocities indicate that the central part of the Potwar Plateau is currently slipping to the S–SE at rates of 3–5 mm/y (e.g. Jouanne et al., 2014, Fig. 1b). These velocities are lower than those estimated from geological evidence for the Late Cenozoic, which are ~8.4 mm/y for the last 12 to 2 My (e.g. Baker et al., 1988; Mcdougall and Khan, 1990, Fig. 2a, Table Ai-ii in supplementary materials). No shortening rates have been estimated for the Potwar Plateau on the thousands of years' time-scale and this lack of information is a major obstacle when discussing the significance of the geodetic velocities in terms of how strain is being accommodated along the salt detachment of the Main Himalayan Thrust (MHT). To fill this gap, overriding active structures, such as those located close to the syntax in the frontal Himalaya of Pakistan (Fig. 1a and b), are appropriate sites for estimating Holocene deformation rates. There, the structural pattern is represented by sub-parallel fault propagation folds related to blind thrusts that accommodate convergence-induced shortening (e.g. Leathers, 1987, Fig. 2b). The most clearly expressed active structure in this area is the Mahesian Anticline (e.g. Nakata et al., 1991, Fig. 3a–c), located in a zone where the salt is ~0.2 km thick (Leathers, 1987, Fig. 1b) and where GPS velocities (India Fixed Reference Frame) are almost zero (<2 mm/y, PK34 station; Jouanne et al., 2014, Fig. 3a). This anticline is bounded to the east by the Jhelum River, which has carved fluvial terraces lying unconformably over Tertiary formations (Siwalik Group; Fig. 4a–e). Some of these terraces have been uplifted by blind thrusts and backthrusts (e.g. Yeats and Lillie, 1991) and are preserved on the E–SE flank of this fold (Fig. 5a–c).

In this contribution, we present the results of a structural and neotectonic survey devised to characterize the structure of the Mahesian Anticline and quantify the Holocene deformation of its SE flank. First, we collected structural data about the orientation of the Tertiary layers of the SE limb of this anticline. Comparing these data with seismic profiles (Leathers, 1987) yields a model of how the leading thrust and backthrust have controlled the structure of the

indicated by a gray scale. GPS velocities of Jouanne et al. (2014) with respect to the India Fixed Reference Frame are represented by red arrows; segmented red rectangles are the dislocations used in their model. InSAR constrained velocities (Chen and Khan, 2010) for the Kalabagh Fault are depicted by blue arrows KF = Kalabagh Fault; SRT = Salt Range Thrust; MBT = Main Boundary Thrust; NPDZ = Northern Potwar Deformed Zone; KA = Khaur Anticline; SS = Soan Syncline; RF = Riwat Fault; BA = Buttar Anticline; TB = Tanwin-Bains Anticline; K = Kallar Anticline; Q = Qazian Anticline; J = Jabbar Anticline; A = Adhi Anticline; BS = Baun Syncline; B = Bhubar Anticline; DA = Domeli Anticline; MA = Mahesian Anticline; LF = Lehri Thrust; DJ = Dil Jabba Thrust; KK = Kotal Kund Syncline; JT = Jogi Tilla Anticline; R = Rhodas Anticline; PH = Pabbi Hills Anticline, MWT = Medlicot-Wadia Thrust, JF = Jhelum Fault, BBF = Balakot-Bagh Fault. (For interpretation of the references to colour in this figure legend, the reader is referred to the web version of this article.)

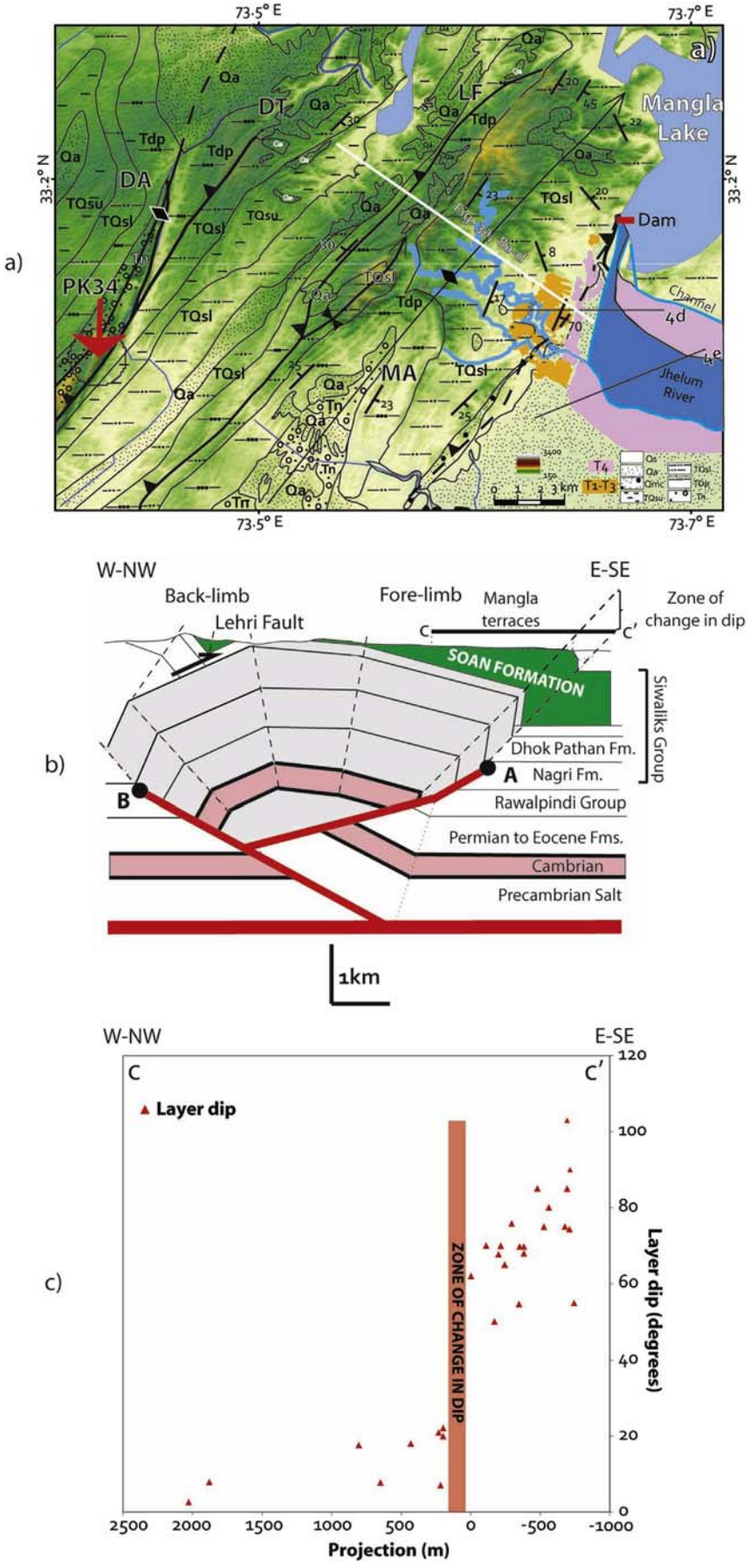
a)
73.5° E
73.7° E
33.2° N
DT
DA
LF
MA
PK34
Mangla Lake
Dam
Channel
Jhelum River
Qa
Tdp
TQsl
TQsu
Tn
T4
T1-T3
3 km
b)
W-NW
E-SE
Back-limb
Fore-limb
Lehri Fault
Mangla terraces
Zone of change in dip
SOAN FORMATION
Siwaliks Group
Dhok Pathan Fm.
Nagri Fm.
Rawalpindi Group
Permian to Eocene Fms.
Cambrian
Precambrian Salt
1km
c)
Layer dip
ZONE OF CHANGE IN DIP
Layer dip (degrees)
Projection (m)

Mahesian Anticline. Second, we mapped four generations of fluvial terraces on its SE flank. Quartz clasts were collected from two levels of terraces for ^{10}Be analysis in order to obtain their exposure ages. We calculate uplift and shortening rates from these ages for a kink-like geometry fold (e.g. Suppe, 1983) which is what we interpret the Mahesian Anticline to be. We compare our thousands of years' time-scale shortening rates with those obtained from geodetic methods in the surrounding area (e.g. Jouanne et al., 2014) and their difference is discussed in terms of the thickness of the salt detachment and its mechanical (creeping and/or stick slip) behavior. We finally propose a conceptual model of how the Mahesian Anticline has grown during the Holocene, as a result of the processes occurring at depth along the MHT. Our results and interpretations seek to evaluate the seismic risk in a region where the ninth largest dam in the world (the Mangla Dam (Fig. 1a and b)) is being constructed.

2. Tectonic and geological setting

The study area is located on the western side of the outermost part of the Hazara-Kashmir Syntax (HKS) in Pakistan (Fig. 1a and b). The HKS is a complex structure in the western Himalaya and corresponds to a bend defined by curved thrust faults whose traces run parallel to each other locally (Bossart et al., 1990, Fig. 1a and b). Its origin has been discussed by Bossart et al. (1990) and it is usually suggested that it started to form during the Pliocene (Treloar et al., 1992). In the HKS, E–W shortening occurred in a portion of the Himalayan belt dominated by N–S convergence (e.g. Coward et al., 1986). The western flank of the HKS is represented by the Potwar Plateau-Salt Range domain (Fig. 1a and b), which is a thin-skinned fold-and-thrust belt above the sub-horizontal salt detachment (e.g. Crawford, 1974). This fold-and-thrust system is bounded to the north by the Main Boundary Thrust (MBT) and to the south by the Salt Range Thrust (SRT) (Fig. 1a and b; Pennock et al., 1989). Its western limit is a lateral ramp, the Kalabagh Fault (Fig. 1a and b; Mcdougall and Khan, 1990), while its eastern limit is the Jhelum Fault, corresponding to the course of the river of the same name (Fig. 1a and b; Baig and Lawrence, 1987). In the Potwar Plateau-Salt Range domain, thrust motion occurs southeastward, parallel to the orientation of the Kalabagh Fault (e.g. Khan et al., 2012). The salt level is the dominant factor controlling the lateral variation of the structural grain in the NW Himalayan fold-and-thrust belt of Pakistan (Khan et al., 2012), and so the locations of the lateral ramps of this plateau—the Kalabagh and Jhelum faults—are probably linked to the extent of these evaporates.

In the vicinity of the Jhelum River, thrusts within the Potwar Plateau-Salt Range have exposed most of the geological units composing this domain. From a mechanical and lithostratigraphic standpoint, the four main units (Gee, 1980, Fig. 2b) are:

i) A Precambrian crystalline basement. This basement crops out only in the Sagortha high, south of the Salt Range. Seismic profiles indicate that its top dips 1°–4° to the north (e.g. Lillie et al., 1987) and that it is affected by normal faults (Grelaud et al., 2002).
ii) A late Precambrian salt layer (Salt Range Formation), which is the main regional detachment (MHT; e.g. Crawford, 1974). It varies in thickness from less than 200 m to more than 3000 m, although these values may not represent the original thickness of the salt, since thickening and thinning related to flow deformation have occurred (Butler et al., 1987).
iii) A Cambrian to Eocene unit of platform deposits. This unit varies in thickness from 200 m to 500 m and mechanically behaves as a "carapace" (Butler et al., 1987). An Oligocene hiatus marks the transition to the overlying molasses (Leathers, 1987).
iv) Miocene to Quaternary syntectonic molasses; these deposits are up to 6 km thick (Mugnier and Huyghe, 2006) and are divided into the Rawalpindi and Siwalik groups (e.g. Anderson, 1927).

3. Deformation rates of the Potwar Plateau-Salt Range

In the eastern part of the frontal Potwar Plateau-Salt Range (Fig. 1a and b), the Salt Range Thrust ends to the NE and the deformation is distributed among several fault propagation folds (e.g. Yeats and Lillie, 1991, Fig. 2b). Seismic profiles show that these structures are led by blind thrust faults rooted in the salt detachment (Pennock et al., 1989) and these thrusts are both foreland- and hinterland-vergent (Yeats and Lillie, 1991, Fig. 2b). The outermost of the recognized fault propagation folds are the Mahesian Anticline, the Rothas Anticline, and the Pabbi Hills Anticline (Fig. 2b).

Numerous deformation rates have been determined for different structures and time-spans between 12 Ma and the present in the Potwar Plateau (e.g. Mcdougall and Khan, 1990; Table Ai-ii in supplementary materials). A synthesis of the structural works performed for the thrusts between the Peshwar Basin and the Salt Range (Fig. 1a and b; Fig. 2a) is proposed here. The long-term mean displacement south of the MBT is deduced from the sum of the incremental displacements of all the recognized structures since 1.8, 2, 4.5, 8, 10, and 11 Ma. Nonetheless, the displacement along the MBT has to be assumed to have been constant between 1.9 and 11 Ma (McDougall et al., 1993) since its temporal distribution is unknown.

Our compilation suggests that tectonic displacement within the Potwar Plateau has occurred at 8.4 ± 0.9 mm/y for the last 11 My (Fig. 2a). This Late Cenozoic mean value is roughly consistent with the 9–14 mm/y obtained farther west by Baker et al. (1988) for the last ~2 My at the front of the Salt Range and with the shortening rates along and south of the Domeli Thrust, located around 10 km northwest of the Mahesian Anticline (Fig. 2b), and constrained at ~7 mm/y for the last 2.5 My (Pennock et al., 1989). However, present-day shortening rates are only 3–5 mm/y (Jouanne et al., 2014) on the central Potwar Plateau and therefore lower than Late Cenozoic rates. This discrepancy between Late Cenozoic and present-day shortening is more obvious on the western (Chen and Khan, 2010) and eastern (Jouanne et al., 2014) borders of the Potwar Plateau–Salt Range (Fig. 1b). Indeed, a GPS station (Jouanne et al., 2014) indicates velocities of <2 mm/y (PK34 in Fig. 3a).

Fig. 3. a) Local structural map of the Mahesian Anticline and its periphery. PK34 is the GPS station of Jouanne et al. (2014). DA = Domeli Anticline, QT = Qazian Thrust; LF = Lehri Thrust, JF = Jhelum Fault. The orientation of the Siwalik beds is also depicted. Profiles of Fig. 4d and e are represented. Tn is the Nagri Formation; Tdp is the Dhak Pathan Formation; TQsl and TQsu are Lower Soan and Upper Soan formations, respectively; Qmc is the Mirpur Conglomerate; Qa are surficial deposits; Qs are stream channel deposits. b) Interpreted structure of the Mahesian Anticline (following Suppe, 1983). Main lithological units are indicated. A and B are the "thrust" and "backthrust", respectively. C-C′ is the profile considered in c). c) Dip of the Siwalik beds from the central part of the Mahesian Anticline to its southeastern most external part. Red triangles depict the slope of the layers projected onto a NW–SE profile. Note the abrupt change in the bed slope, as indicated by the red transparent bar that depicts the kink-like geometry of the anticline. (For interpretation of the references to colour in this figure legend, the reader is referred to the web version of this article.)

4. Structure of the Mahesian Anticline

The Mahesian Anticline is the best expressed active structure on the Potwar Plateau (Nakata et al., 1991) and is composed of folded Tertiary fluvial series (Rawalpindi Group and Nagri, Dhok Pathan, and Soan formations of the Siwalik Group; Fig. 3b; Khan et al., 1997). Its axis dips to the NE and the fold is ~20 km long and 6 km wide (Fig. 3a and b). Seismic lines (Leathers, 1987) indicate that the Mahesian Anticline developed above the detachment at the base of the salt formation at a depth of ~4 km (e.g. Leathers, 1987). It is mainly the result of a hinterland-vergent blind thrust although some foreland-vergent blind thrusts (Yeats and Lillie, 1991) and detachments within the Tertiary piles (Grelaud et al., 2002) make the structure more complex (Fig. 3b). Lateral variations also affect its geometry.

A structural analysis along the profiles in Fig. 4b and c and Fig. 5, close to the seismic line PTW1 (Leathers, 1987), indicates that beds dip at less than 20° close to the fold axis, while they dip at more than 60° on the outermost part of the SE flank, where they may even be subvertical (Fig. 3c). The change in the dip of the Siwalik layers from the inner part of the SE flank to its outermost part is abrupt (Fig. 3b and c) and suggests a kink-like geometry (Suppe, 1983). A strongly tilted unconformity between the Quaternary sediments and the Siwalik layers indicates rotation of the SE flank during the formation of the anticline (Fig. 5c). The structural development of the Mahesian Anticline is discussed further in section 7.

5. Fluvial terraces on the SE flank of the Mahesian Anticline

Four generations of fluvial terraces have been distinguished on the SE flank of the Mahesian Anticline (Fig. 4a–e; Fig. 5a–c). They are formed from fluvial conglomerates deposited unconformably over the Siwalik (Fig. 6a and b). We have named these terraces T1 to T4 from oldest to youngest, respectively. The most developed terrace is T2, which was mainly formed by a paleo-meander of the Jhelum River; remnants of sediment of the paleo-Jhelum River terrace are found spatially related to T2 and are assigned to the T1 terrace. Terrace T3 is linked to the incision of the Baral and Pandori tributaries into terraces T2 and T1 (Fig. 4a). Since the development of terraces along the two tributaries was not necessarily synchronous, we focus on the terraces constructed by the Baral Tributary in what follows. Terrace T4 was cut by the Jhelum River. The deposits associated with T1 are more than 10 m thick, while the deposits related to terraces T2 and T3 are less than 4.5 m and 2.5 m thick, respectively.

We performed satellite image analysis and Aster GDEM topographic profiles around the Jhelum River, from the periphery of the Mahesian Anticline to its intersection with the Pabbi Hills Anticline (Fig. 3a, Fig. 4d and e). We measured the terrace elevation with respect to the WGS84 ellipsoid, with a precision of ±0.1 m, by performing DGPS topographic leveling (Fig. 4b and c). Close to the dam, the anthropic effects due to its construction are substantial and preclude a detailed topographic study along the northern part of T4 (Fig. 4a). Furthermore, construction of a high resolution DEM was not possible due to restrictions on movement in this military area; so elevation data of the terraces were simply projected on NW–SE cross-sections (Fig. 4b and c).

The top of T1 is poorly preserved and its geometry is not discussed further here. T2 is nearly flat and at an elevation of nearly 300 m in its northwestern part whereas its southeastern part is tilted eastwards and its elevation less than 250 m (Fig. 4b and c). This tilting occurs above the steep Siwalik beds (Fig. 4b and c, bottom). Along the Baral River, T3 is also tilted westward above the steep beds of the fold and its elevation varies between 283 m and 256 m (Fig. 4b and c, bottom). At the intersection between the Baral and Jhelum rivers, T4 is ~10 m above the river bed and was reached by catastrophic high flow prior to the dam's construction. Its northern part is higher than the river, even after its excavation during the dam construction, so this zone was probably affected by fold warping. The overall geometry of T2 and T3 indicates homogeneous uplift of the northeastern part of the terraces and tectonic tilting above the steep beds of the southeastern flank of the Mahesian Anticline (Fig. 4b and c).

The incision of this zone is controlled by the uplift of the Mahesian Anticline and the consequent changes in the geometry of the river. The uplift of the Mahesian Anticline since the construction of T1 has promoted the eastward migration of the Jhelum River bed to its present day position and locally favored incision. River trend changes have been documented as a significant control in the incision rate, for instance, further east along the Himalaya, in the Darjiling sub-Himalaya. There, the Tista River, obeying to an augmentation in deformation rates along out-of-sequence reverse faults, has migrated and strengthened its incision (Mukul et al., 2007).

Nonetheless, south of the Mangla Anticline, the Jhelum River is locally anastomosed and only incises T4, whereas no clear incision between T4 and older features is evidenced. There, the vertical incision between the low stand of the Jhelum River and T4 is less than 10 m and reflects the dynamics of the river between low flows and catastrophic high flows (Fig. 4d and e). A stable level of the Jhelum River is therefore inferred during terrace construction. Furthermore, the slope of the Jhelum River is less than 0.1%; thus, the difference in elevation compared to the initial slope of the river between the downstream and upstream parts of T4 is only a few meters. Therefore, the difference between the tops of terraces T4 and T2 is thought to reflect the uplift. This results in an uplift of 60 ± 5 m for the northwestern T2 site (i in Fig. 4a).

The watershed areas of the tributaries are both around 10 km^2 and their evolution is controlled by changes in the Jhelum River. The abandonment of the T2 meander by the Jhelum River increased the length of the Baral tributary by ~30% (3 km versus 10 km). This means its present-day elevation above the Jhelum River is greater than its elevation during the development of T3. Therefore, the difference between the tops of terraces T4 and T3 is thought to underestimate the uplift. Nonetheless, the present-day slope of the Baral River is uncertain given the existence of a small dam along its course and is estimated at between 0.4 and 0.8% (Fig. 4b and c); these uncertainties are used to estimate the uplift component for the northwestern sites of T3 as 37 ± 5 m (iii in Fig. 4a).

6. ^{10}Be concentrations and age interpretation

Cosmogenic radionuclides (CRN) have been successfully used to constrain the age of deformed geomorphic surfaces (e.g. Frankel et al., 2015). These isotopes are generated within the first few meters of the Earth's surface due to the impact of secondary cosmic rays; their production rate decreases exponentially with depth (Lal, 1988). At a given depth (x) and for a material density (ρ), the production rate (P_x) can be estimated if the surface production rate (P_0) is known (Lal, 1991):

$$P_x = P_0 e^{-(x\rho/\Lambda)} \quad (1)$$

where Λ is the characteristic attenuation factor, which is roughly invariant at different locations on Earth (Lal, 1991).

In situ produced CRN (here ^{10}Be) can be used to measure the duration of surface exposure to cosmic rays (cf. Gosse and Phillips, 2001) and so provides a numerical age for a surface. These ages must be considered apparent because they are dependent on

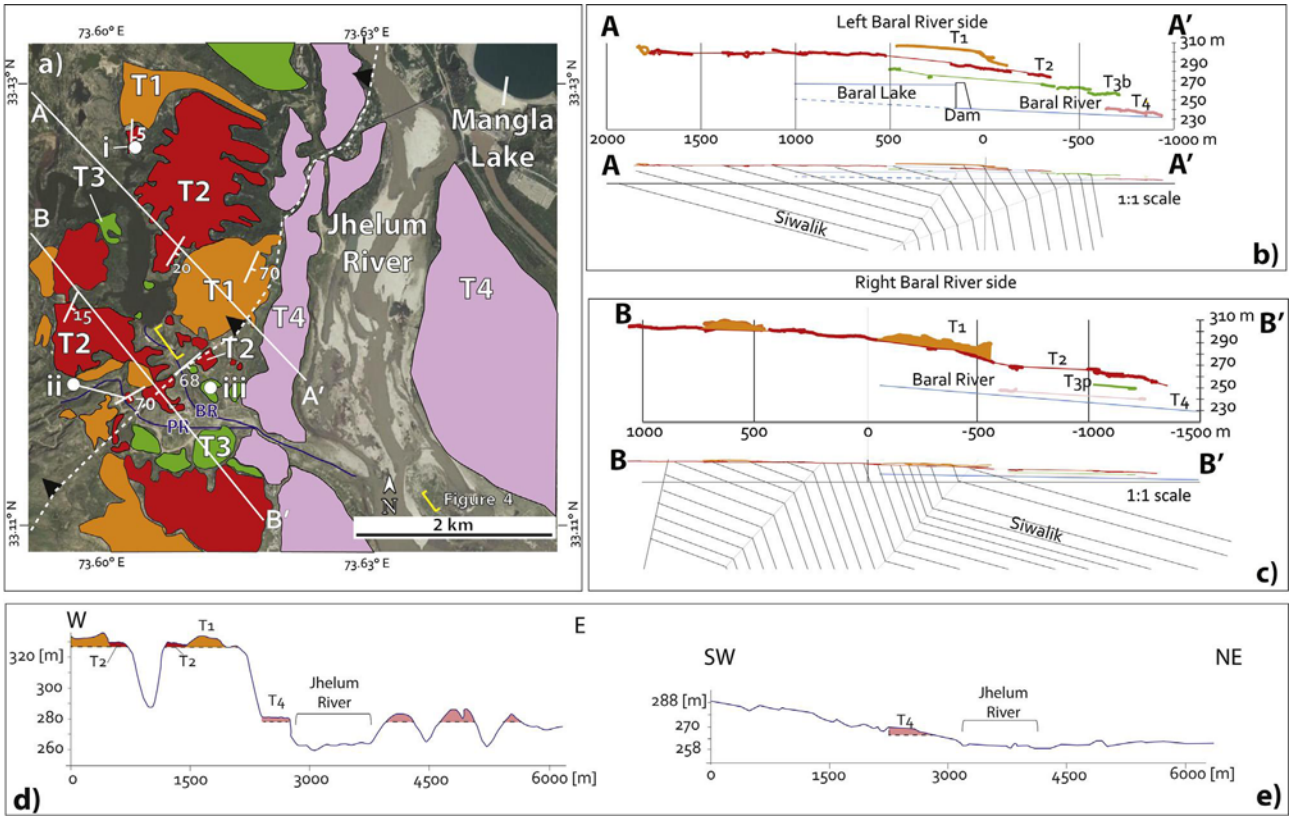

Fig. 4. a) Map view of the terraces on the Mahesian Anticline in a Google Earth image. i, ii and iii are the ^{10}Be sample sites. White solid lines AA′ and BB′ are the projected DGPS profiles shown in b) and c). BR and PR are the Baral and Pandori rivers, respectively. b) and c) are, in the upper sections, the profiles AA′ and BB′, respectively. Terraces of the left and right sides of the Baral River were respectively projected. The lower sections of b) and c) show the relation between the terraces and the change in dip of the Siwalik across the Mahesian Anticline. T3b and T3p, are the terrace T3 produced by the Baral and the Pandori tributaries, respectively. d–e) Topographic profiles of Fig. 3a from Aster GDEM.

parameters including prior exposure issues (inheritance, e.g. Anderson et al., 1996), post-depositional effects (partial shielding, e.g. Putkonen and Swanson, 2003), and erosion (e.g. Brown et al., 1991). Considerations about additional parameters, sample preparation procedures, and laboratory facilities are addressed in supplementary materials.

In this study, the ages obtained correspond to the abandonment of fluvial terraces as a consequence of the formation of the Mahesian Anticline. Only T2 and T3 were sampled (Fig. 6a–h). Much of the original surface of terrace T1 is occupied by a military camp and access is prohibited, while elsewhere the surface has been largely obliterated by natural incision(s) post-abandonment, resulting in a rough surface from which it was not possible to select appropriate sample sites. No suitable sites were identified for T4 because it has been disturbed by anthropic action. To determine exposure ages, we collected boulders and pebbles both from the surfaces of these terraces and along vertical profiles. We chose to collect quartz fragments exclusively in order to analyze samples with the same lithology (Fig. 7a). Gneisses and granites were too scarce or too badly weathered to be suitable for this kind of analysis. In order to estimate the amount of inherited ^{10}Be due to prior exposure processes of the clasts, samples (one per depth level) were collected from around 2.5 m deep in terraces T2 and T3, following the strategy of Anderson et al. (1996).

The pebbles come from the Himalayan Belt, located approximately 100 km to the north, while the boulders originate from the Siwalik that crops out in the study area. Samples are assumed not to have been remobilized after their deposition in the terrace sediments because of the well-preserved fluvial sorting. Cosmogenic ages for similar fluvial terraces in NW Himalaya have resulted in ages of ~30 ka or younger (e.g. Bookhagen et al., 2006). For such a period only strong surface denudation (>1 m) would significantly affect the exposure ages. The aspect of terraces T2 and T3 is dominantly flat (Fig. 6c, f), which suggests a very low denudation rate, meaning this parameter can be ignored for age calculations. We test anyway maximal erosion rates to evaluate its incidence in age calculations. Thirteen samples were obtained from two sites on terrace T2 (i and ii in Fig. 4a; Fig. 6c–e) and seven samples from one site (iii in Fig. 4a; Fig. 6f–h) in terrace T3. Table 1 shows the details of each sample.

Four surface samples from terrace T2 give a coherent average ^{10}Be concentration of ~37 000 ± 4800 at/g (Fig. 7a). Sample PK2007-09 (orange diamond in Fig. 7a) has a high ^{10}Be concentration (~63 000 at/g), possibly largely due to inheritance. Probably, this high inheritance is due to its size (1.2 m in diameter) and the occurrence of Siwalik outcrops in the catchment of the Pandori River. Thus, the boulder is too big to have been effectively transported by this tributary. Data obtained at depth show a significant scattering in terms of ^{10}Be concentration (Fig. 7a). They do not fit any curve of ^{10}Be decreasing concentration with depth, suggesting a potential inherited amount of this isotope variable from one clast to another (Fig. 7a). If this is correct, the samples with the lower inheritance are those with the lowest concentration of ^{10}Be both at the surface and at a given depth. Even if it has been suggested that sampling sand may give less scattered results (Hidy et al., 2010), other studies demonstrate that both sand and coarser samples may result in considerable dispersion of ^{10}Be concentration data (e.g. Rizza et al., 2015; Oskin et al., 2008). Based on this, we consider it unlikely that the observed scattering is conditioned by the size of the collected samples.

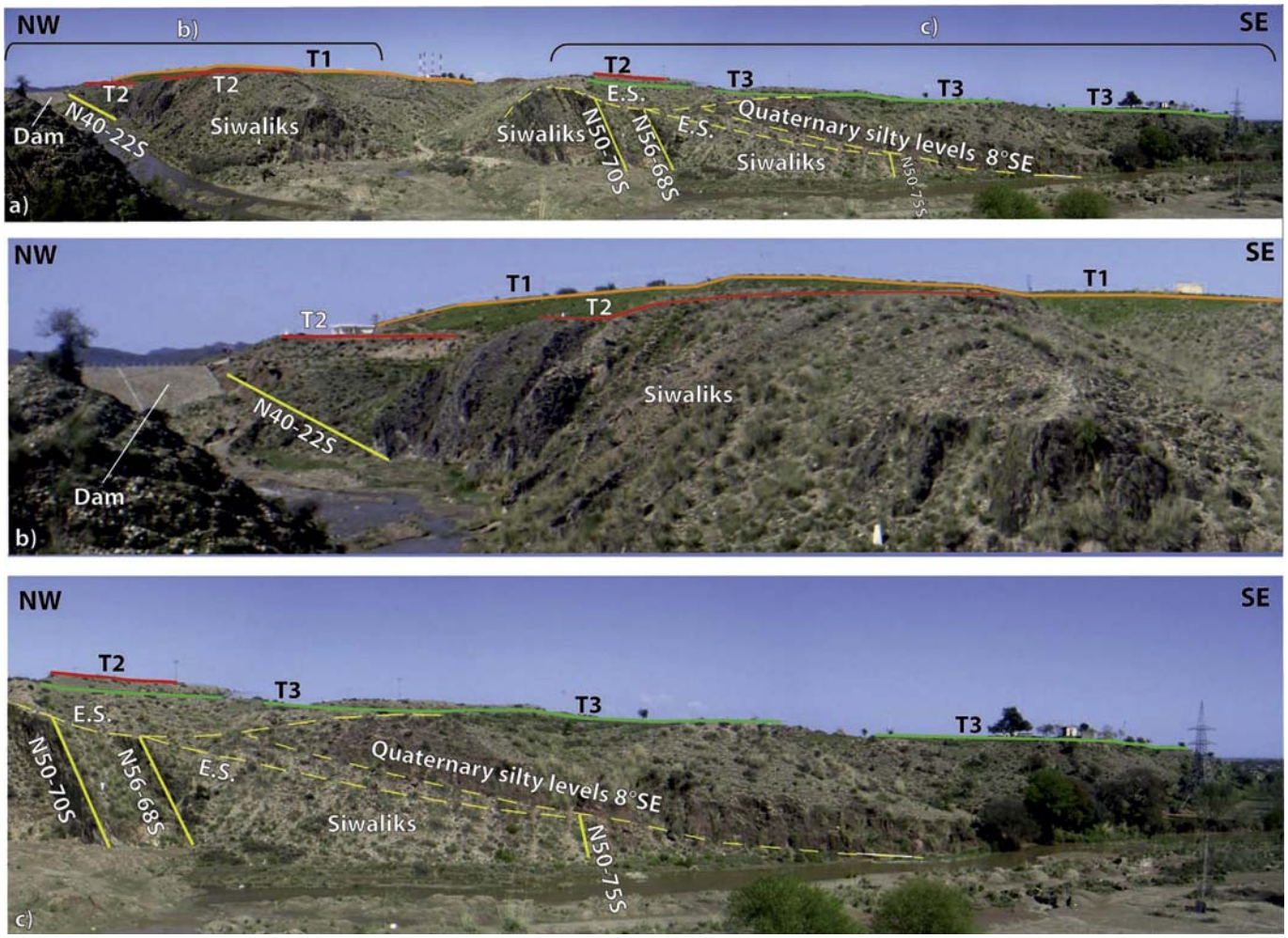

Fig. 5. a) Panoramic view of the SE flank of the Mahesian Anticline. b) Detailed view of beds pertaining to the Siwalik Group along the Baral River. The dips of the layers are gentle (~20°) beneath the irrigation dam. c) Detailed view of the layers of the Siwalik Group in the easternmost part of the Mahesian Anticline. Subvertical (~70°S) beds of the Siwalik are observed. Terraces T1 to T3 are depicted by colored lines. Yellow continuous lines are the Siwalik beds. Yellow segmented lines are silty levels overlying the Siwalik beds. (For interpretation of the references to colour in this figure legend, the reader is referred to the web version of this article.)

For T2, zero erosion was first assumed for the calculations. Next, we developed a least square calculation, which is a function of the exposure age and inheritance, to generate a curve that confirms the production rate attenuation law of Lal (1991), considering the two least concentrated samples at the surface and at depth, PK2007-23 and PK2007-28, with their uncertainties (red curve in Fig. 7a). In Fig. 7a, the samples to the right of the curve contain higher inheritance than those located on the curve; therefore, the model represents the maximum age with the minimum inheritance. With this, we obtained a maximum age of 6.5 ± 0.2 ka for terrace T2. To test the influence of erosion in our estimations, we secondly considered a maximum erosion rate of 0.018 mm/y, which has been suggested for Bhutan terraces (Berthet et al., 2014), in a much wetter area. With this, we observed that the zero erosion age is not modified by more than 600 y. Hence, even with this unlikely erosion rate, our results are not significantly affected. We thus consider our zero erosion age as reliable and in agreement with the age of a cool and dry climatic period in NW Himalaya reported at 7.7 to 6.1 ka (Trivedi and Chauhan, 2009), conducive to the abandonment of fluvial terraces.

For terrace T3, the same reasoning and methods are followed (Fig. 7b). Assuming an erosion rate of zero, the calculated ^{10}Be concentration is consistent with a maximum age of 3.3 ± 0.7 ka, which is coherently younger than the maximum age of terrace T2 (Fig. 7b). We also tested a 0.018 mm/y erosion rate and observed that the estimated age is not greatly affected (<200 y). The estimated maximum age for T3 is similar to other Holocene terraces in the Himalaya and can be correlated with a cool and dry climate stage in the NW Himalaya from 4 ka to 2 ka (Trivedi and Chauhan, 2009).

7. Holocene deformation rates of the Mahesian Anticline

Considering the abandonment age of the terraces and their uplift, the uplift rates for the Mahesian Anticline are between 9.2 ± 0.8 mm/y and 11.2 ± 2.8 mm/y, respectively, for terraces T2 and T3; given the uncertainties, an uplift rate of ~10 mm/y is considered in the following. Tilting above the southeastern flank of the anticline is occurring at a rate of ~0.5%/ky, a value that suggests a Late Pleistocene age for the unconformity that dips 8° at the boundary between the terrace deposits and Siwalik beds (Fig. 5c). This tilting is linked to shortening of the Mahesian Anticline, as described in the following section.

Previous works about the Mahesian Anticline (e.g. Leathers, 1987) claim that the deformation of the sedimentary pile is due to the effect of two blind thrusts within the core of the detachment

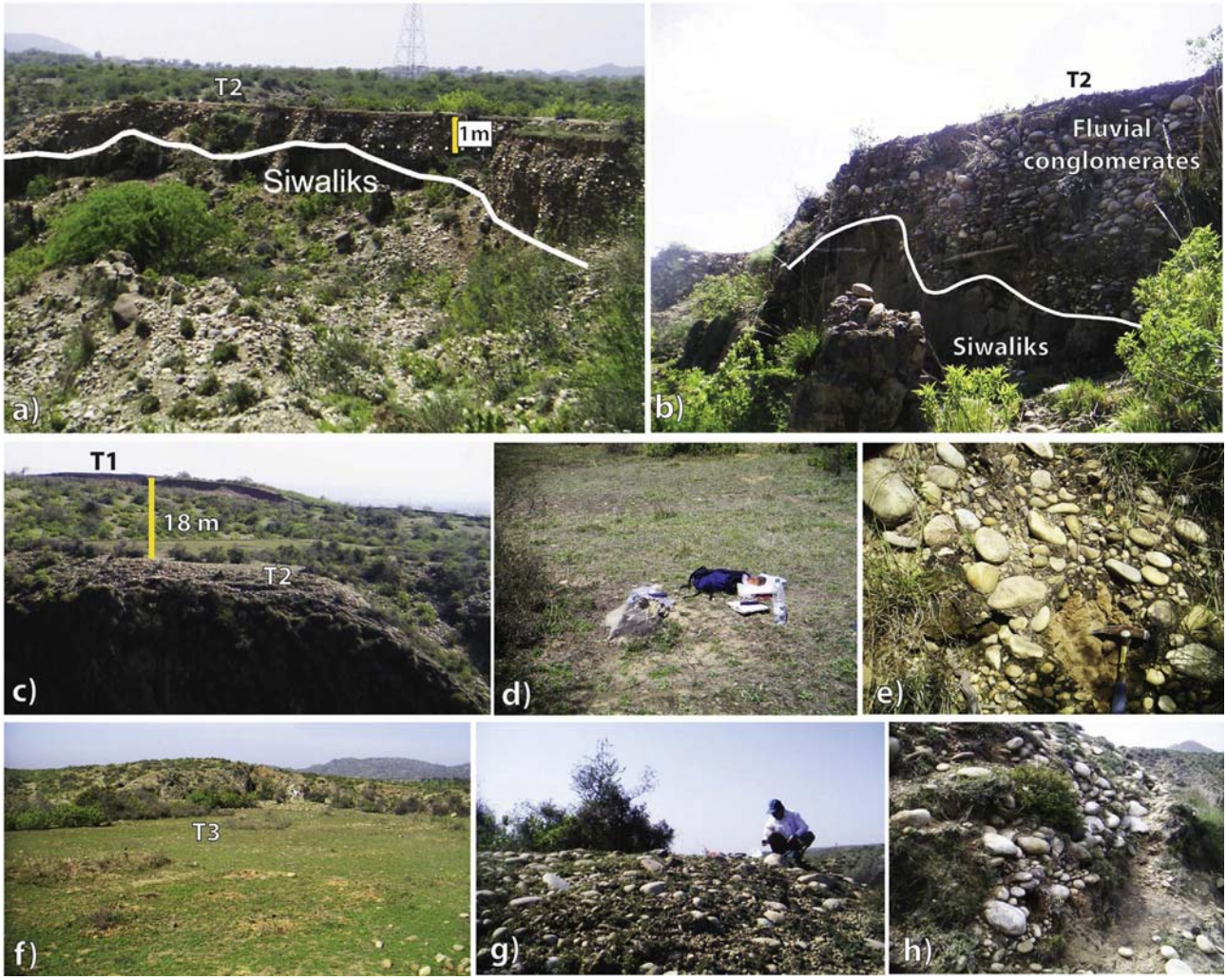

Fig. 6. Field photographs of the fluvial terraces of the Mahesian Anticline. a–b. Fluvial conglomerates beneath terrace T2 in discordance over the Siwalik deposits (site i). White lines in a) and in b) represent the discordance. c) General view of terraces T1 and T2. d) Detailed view of the surface of terrace T2 (site ii). e) View of the section where clasts for the ^{10}Be profile for T2 were collected. f) General view of terrace T3. g) Detailed view of clasts over terrace T3. h) View of the section where clasts for the ^{10}Be profile for T3 were collected.

fold: a foreland-vergent thrust and a hinterland-vergent backthrust (Fig. 8). The genetic link between the fold and the two faults is unclear and the different seismic profiles indicate that their respective influence varies laterally. The whole anticline seems to be a truncated detachment fold (Wallace and Homza, 2004), although the tilting observed above the steep beds suggests a trishear fault-propagation fold (Erslev, 1991).

In what follows, the homogeneous uplift rate (U) of the north-eastern part of the terraces is considered as the first-order parameter for characterizing the Holocene deformation of the Mahesian Anticline. The simplifications suggested by Grelaud et al. (2002) were used to analyze the fold by adapting the equations of Mugnier et al. (2006).

Above a ramp, the displacement is parallel to the underlying fault segment if this latter is considered fixed (Avouac, 2003) and is expressed by:

$$U = V^{*}\sin a \qquad (2)$$

where U is the uplift rate above the ramp, V the shortening rate, and α the dip angle of the causative ramp (Fig. 8). In the case of a flat parallel to the beds and a backthrust ramp, a basal wedge is defined between the basal décollement and the ramp. Assuming the displacement is zero at its front, the slip along the ramp is equal to the slip along its base, and Equation (2) still applies for estimating the velocity above the wedge.

However, a zig-zag pattern is proposed for the faults within the core of the Mahesian Anticline: a steep backthrust roots into the salt detachment at ~4 km depth whereas a gentle thrust is connected to the backthrust (Fig. 8). The uplift of the fold is therefore the sum of the contribution of the two faults, and six domains, bounded by faults or axial active surfaces. Above the faults, two trishear propagating zones bound the central part of the anticline and develop at the tip of the thrust and back-thrust (Fig. 8); the footwall of the faults is formed by the back-stop and the foreland zone where a wedge is also formed between the backthrust and the thrust (Fig. 8a).

For the central domain above the superposed faults (violet zone in Fig. 8), the total uplift Ut is the sum of the uplift U induced by the backthrust (Equation (2)) and additional uplift (U_a) related to the thrust. This additional uplift component U_a is also determined from Equation (2) when slip along the thrust (dip α') is estimated (Fig. 8). The attenuation of displacement between the backthrust and thrust is weak as the hanging-wall cut-off angles are small (Suppe, 1983) and we have:

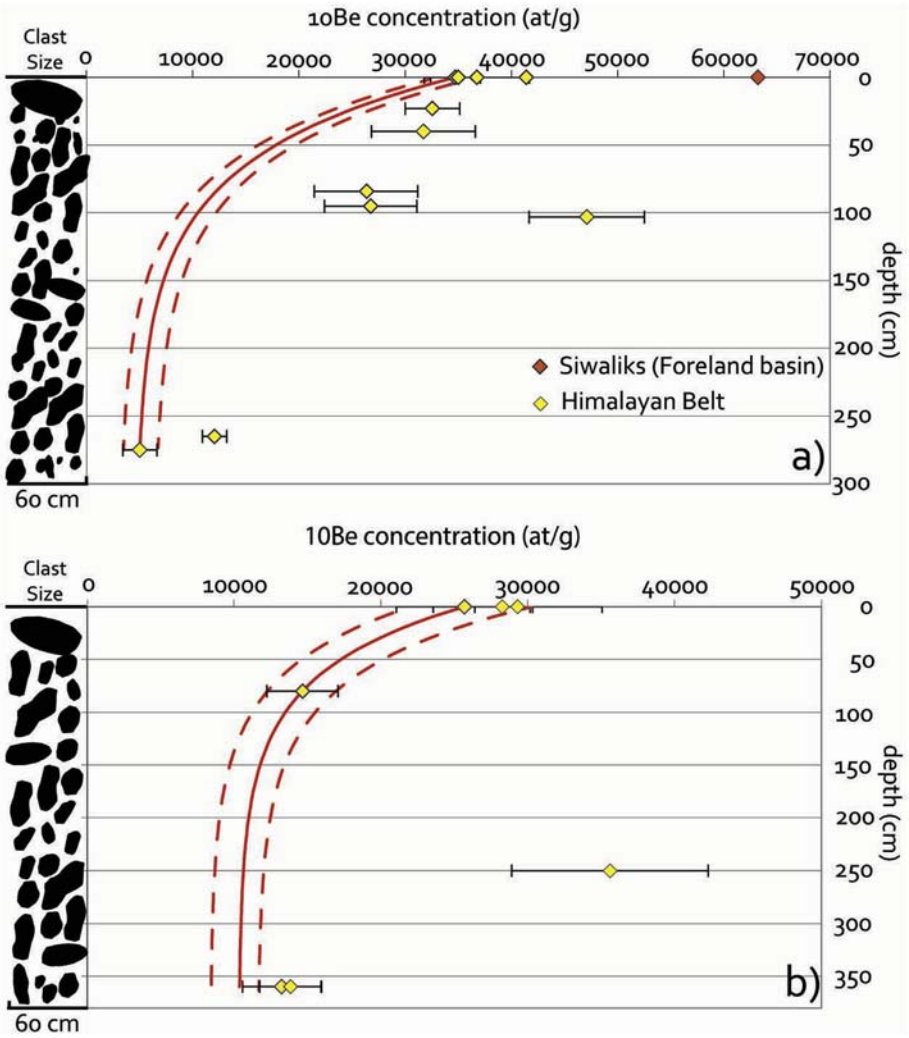

Fig. 7. Concentration of ^{10}Be versus depth profiles for a) Terraces T2 and b) Terrace T3. Red curve is the inversion model following Vassallo et al. (2015). The red segmented lines are given by the uncertainties associated with both surface and in-depth less concentrated samples. Yellow and red diamonds indicate Siwalik and Himalayan Belt clasts, respectively. (For interpretation of the references to colour in this figure legend, the reader is referred to the web version of this article.)

$$Ut \sim V(\sin\alpha + \sin\alpha') \quad (3)$$

From Equation (3), the shortening rate would be 14 mm/y for the geometry proposed in Fig. 8 ($\alpha = 30°$ and $\alpha' = 15°$); for the steepest fault system that can be inferred (e.g. $\alpha = \alpha' = 30°$), the shortening would be 10 mm/y.

The former analysis suggests that the Holocene shortening rate for the Mahesian Anticline is greater than the regional long-term 8.4 mm/y rate. The rate obtained for the Mahesian Anticline is probably affected by the local E–W shortening (Coward et al., 1986) that enhances deformation in the core of the syntax and is not related exclusively to the present-day regional shortening.

Due to an unknown component of strike-slip motion that could affect the Mahesian structure and the complexity of the kinematics of the whole syntax, no attempt is made to estimate this contribution.

8. Discussion: deformation of the Potwar Plateau

We have estimated shortening rates for the Mahesian Anticline at the Holocene timescale. Our estimations are in general consistent with geologically constrained deformation rates and lower than instantaneous velocities. In this section we first discuss how deformation conducted by thrusts and backthrusts in the Potwar Plateau has evolved (in-sequence or out-of-sequence activity). Then, we argue about how the variable salt thickness along the MHT under the plateau seems controlling the spatial Holocene-instantaneous deformation pattern. Finally, we discuss about the mechanical behavior along the MHT depending on the thickness of the salt horizon; this latter aspect helps in assessing the seismic hazard for a region in which no historical Mw $\geq$ 6 earthquakes have been documented.

8.1. Late Cenozoic versus Holocene deformation rates

The slightly greater Holocene shortening rate of the Mahesian Anticline is consistent with the Late Cenozoic 8.4 mm/y regional estimation for the Potwar Plateau (Fig. 2a). In particular, it is close to the 9–14 mm/y shortening rates provided by (Baker et al., 1988) for the last 2 My for the frontal Salt Range. Therefore, we suggest that deformation of the NE Potwar Plateau has been mainly concentrated in the Mahesian Anticline during the Holocene. This is in agreement with the regional interpretation of Jouanne et al. (2014), which states that deformation along the MHT is essentially

Table 1
^{10}Be data. See the supplementary materials for details about sample preparation and laboratory facilities. i, ii, and iii indicate the specific sample sites in each terrace.

Sample	Terrace	Lat (°)	Long (°)	Elevation (m)	Depth (cm)	^{10}Be concentration (at/g)	Uncert (at/g)	Shielding factor	Surface production (at/g/y)	Size cm	Facies	Comments
Pk2007-23	T2(i)	33.125°	73.605°	323	0	34,734	2337	1	4.7	15	Quartz	Whole pebble
Pk2007-24	T2(i)	33.125°	73.605°	323	0	36,762	4951	1	4.7	30	Siwalik	Fragments from the upper face
Pk2007-01	T2(ii)	33.103°	73.605°	307	0	41,410	4559	1	4.7	60	Quartz	Fragments from the upper face the upperface the upper face
Pk2007-09	T2(ii)	33.103°	73.605°	307	0	63,216	2653	1	4.7	30	Siwalik	Fragments from the upper face
Pk2007-11	T2(ii)	33.103°	73.605°	307	0	35,021	7506	1	4.7	20	Quartz	Fragments from the upper face
Pk2007-06	T2(ii)	33.103°	73.605°	307	30	94,544	12,014	1	4.7	10	Quartz	Whole pebble
Pk2007-26	T2(i)	33.125°	73.605°	323	40	31,721	4889	1	4.7	15	Siwalik	Whole pebble
Pk2007-25	T2(i)	33.125°	73.605°	323	45	32,576	2552	1	4.7	7	Siwalik	Whole pebble
Pk2007-07	T2(ii)	33.103°	73.605°	307	84	26,391	4875	1	4.7	11	Siwalik	Whole pebble
Pk2007-27	T2(i)	33.125°	73.605°	323	95	26,756	4347	1	4.7	10	Siwalik	Whole pebble
Pk2007-08	T2(ii)	33.103°	73.605°	307	103	47,105	5451	1	4.7	10	Quartz	Whole pebble
Pk2007-32	T2(i)	33.125°	73.605°	323	265	12,052	1146	1	4.7	10	Quartz	Whole pebble
Pk2007-28	T2(i)	33.125°	73.605°	323	275	5040	1616	1	4.7	substratum	Siwalik	Fragments from the upper face
Pk2007-12	T3(iii)	33.103°	73.613°	294	0	29,311	5750	1	4.7	100	Siwalik	Fragments from the upper face
Pk2007-13	T3(iii)	33.103°	73.613°	294	0	25,701	4648	1	4.7	40	Murree	Fragments from the upper face
Pk2007-14	T3(iii)	33.103°	73.613°	294	0	28,281	1885	1	4.7	40	Murree	Fragments from the upper face
Pk2007-17	T3(iii)	33.103°	73.613°	294	80	14,663	2427	1	4.7	20	Siwalik	Fragments from the upper face
Pk2007-18	T3(iii)	33.103°	73.613°	294	250	35,603	6699	1	4.7	15	Quartz	Whole pebble
Pk2007-20	T3(iii)	33.103°	73.613°	294	360	13,251	2676	1	4.7	0.1	Quartz	Amalgamated sand
Pk2007-21	T3(iii)	33.103°	73.613°	294	360	13,857	2120	1	4.7	15	Quartz	Whole pebble

transferred to the Salt Range Thrust.

The eastern boundary of the Potwar Plateau is represented by the Jhelum Fault, which is an active fault as deduced from its seismicity, old linear landslides, and deflected drainages (Baig and Lawrence, 1987). The evolution of this long-lived fault is complex and no estimations of its slip rates have yet been determined. Because the Mahesian Anticline is on the western side of the Jhelum Fault, we suggest that the Jhelum Fault is, for recent periods, a sinistral fault transferring shortening to our targeted frontal structure.

Considering previous works and our results, we suggest that the active fault systems within the western part of the HKS are represented by the Kalabagh Fault, the Salt Range Thrust, the Mahesian Anticline, and the Jhelum Fault (red lines in Fig. 9a and b). Therefore, in-sequence deformation dominates in the NE Potwar Plateau during the Holocene. Out-of-sequence thrusts are more active eastwards, as evidenced by Vassallo et al. (2015), who suggest that deformation is accommodated between the Medlicott-Wadia Thrust and the MFT.

8.2. Present-day versus Holocene deformation rates

Present-day deformation of the Potwar Plateau was measured between 2006 and 2012 by deploying temporal GPS stations (Jouanne et al., 2014). The obtained data are not affected by increased stress during and after the 2005 Mw 7.6 Kashmir Earthquake (Parsons et al., 2006). Deformation field has been modeled by supposing the MHT as a set of dislocations within an elastic half-space (red dashed boxes in Fig. 1b). At the surface, these dislocations reproduce a velocity field that increases southwards (red vectors in Fig. 1b; Jouanne et al., 2014).

On the western side of the plateau, the analysis of InSAR images acquired between 1992 and 1999 (Chen and Khan, 2010) indicates that the creep component of the slip along the Kalabagh Fault is around 5.7 mm/y in its northern section, and decreases to its southern termination where the slip is less than 3.7 mm/y (Chen and Khan, 2010; blue vectors in Fig. 1b). This fault accommodates a lesser amount of instantaneous deformation in a zone where the salt thickness tapers (southern tip, Fig. 1b). Similarly, the salt thickness decreases towards the Jhelum Fault and the instantaneous deformation close to this fault is almost zero (PK34 station, < 2 mm/y, Jouanne et al., 2014, Fig. 3a). We emphasize that the present-day slip rates in the central Potwar Plateau (Jouanne et al., 2014) are lower than all the reported geological rates, including our Holocene results. Furthermore, geodetic velocities provided for the eastern and western Potwar Plateau differ markedly from our Holocene rates. We surmise that this lateral decrease in the instantaneous velocities is controlled by the thinning or absence of the salt level.

8.3. Creep pulses triggered by increased deviatoric stress?

It is widely accepted that deformation of the Potwar Plateau is induced by aseismic slip on a viscous detachment represented by the salt level (e.g. Seeber and Armbruster, 1981). However, the discrepancy between Holocene and instantaneous deformation rates on the lateral borders of the Potwar Plateau imposes substantial constraints on this assumption. From a mechanical standpoint, two possibilities are proposed to explain this difference (Fig. 9a and b).

The first possibility is based on the properties of the salt level. From creep experiments performed on rock salt (e.g. Urai et al., 2008), it is found that dislocation creep rates (ε_{DC}) evolve according to the differential stresses ($\sigma1 - \sigma3$), as depicted by Equation (4).

$$\varepsilon_{DC} = Ae^{\frac{-Q_{DC}}{RT}}(\sigma1 - \sigma3)^n \quad (4)$$

where A is a constant of the material properties, Q_{DC} the activation energy for dislocation creep, R the gas constant, T the absolute temperature, σ1 and σ3 are the maximum and minimum stresses, and n is a stress exponent. For salt, n varies from 3 to 6, with greater values at higher stresses (Hunsche and Hampel, 1999).

The velocity (V) of the sedimentary carapace of the Potwar Plateau is linked to the deformation rate of the underlying salt level, and assuming a homogeneous simple shear deformation it is found (Coward and Kim, 1981) that:

$$V = 2\varepsilon\ H \quad (5)$$

with H being the thickness of the salt level and ε the component of pure shear strain rate.

Assuming that the creep rates and the pure shear strain rate component are equal, combining Equations (4) and (5) indicates that:

$$V = 2\ Ae^{\frac{-Q_{DC}}{RT}}H(\sigma1 - \sigma3)^n \quad (6)$$

Equation (6) is a simplification of how deformation is accommodated, but it indicates that the velocity of the sedimentary carapace is conditioned both by the thickness H of the salt level and the deviatoric stress (σ1 - σ3).

This thickness control inferred from the above law is confirmed: the decrease in the present-day velocity of the southern Kalabagh Fault spatially correlates with zones of thin salt (Chen and Khan, 2010, Fig. 1b). Similarly, the eastern termination of the Potwar Plateau, where the lowest geodetic slip rates have been determined (Jouanne et al., 2014, Fig. 1b), is also located above a zone where the salt is thin (<0.2 km thick). In contrast, the highest GPS velocities are observed in the central zones of the Potwar Plateau-Salt Range domain, where the salt is thicker than 1.8 km (Fig. 1b).

Assuming that salt creeping is the only deformation-inducing process, the contrast between Holocene and present-day velocities in the Potwar Plateau implies that the creep rate used to be faster than that currently observed by Jouanne et al. (2014). Equation (6) indicates that creep may be accelerated if deviatoric stresses rise. Earthquakes like the ~25 AD Taxila event (Fig. 1a; Fig. 9a), which is believed to have occurred at the NW hinterland limit of the Potwar Plateau (Ambraseys et al., 1975), along the deeper and presently locked part of the MHT (Jouanne et al., 2014), may increase the deviatoric stress controlling creeping, making it faster (Fig. 9a). The repetition of such earthquakes supposedly induces bursts of intense creeping, in addition to the regular creep rates. Moreover, the occurrence of such bursts is thought to enhance the long-term deformation of the Potwar Plateau at rates higher than those recorded nowadays with geodesy.

The second possible explanation for the lateral velocity contrast is to suppose an asperity locally induced by tectonic thinning of the salt detachment that creates areas without salt. A similar asperity nucleated the 1992 Mw 6 earthquake that struck the Kohat Plateau area (Satyabala et al., 2012, Fig. 1a), a region formerly assumed to be of low seismic risk. There, geodetic velocities are also lower than the geological shortening rates (Satyabala et al., 2012). This event suggests stick-slip mechanical behavior occurring locally along the detachment.

From this analogy, the contrast between our data and the geodetic velocities in the Potwar Plateau area could be linked to irregular tectonic thinning of the salt detachment (Fig. 1b). This irregular pattern has been already evidenced (Fig. 1b) and may be due to normal faults that offset the salt level and promote the accumulation of salt in the core of folds (Grelaud et al., 2002). Intense thinning of the salt level between the anticlines is believed to create asperities that lock the main detachment, accumulate elastic strain (Cotton and Koyi, 2000), and suddenly release it during earthquakes. The anticlines of the eastern border of the Potwar Plateau (Fig. 9b) are positioned over a zone where the salt is thinner and irregular (Fig. 1b; Leathers, 1987). Therefore, we suggest stick-slip behavior occurs in the zone east of the dislocation that currently creeps beneath the central Potwar Plateau (red box in Figs. 1b and 9b).

8.4. Large earthquakes beneath the eastern Potwar Plateau?

The hypothesis involving earthquakes in the study area contradicts the aseismic character of the MHT underneath the Potwar Plateau (Fig. 9b), usually inferred from the absence of historical Mw ≥ 6 earthquakes for the past several centuries (Monalisa et al., 2009). Nevertheless, instrumental data show that seismic activity in that area is represented by Mw < 5 earthquakes and a few Mw 5 earthquakes (Monalisa et al., 2009, Fig. 1a). This suggests that the

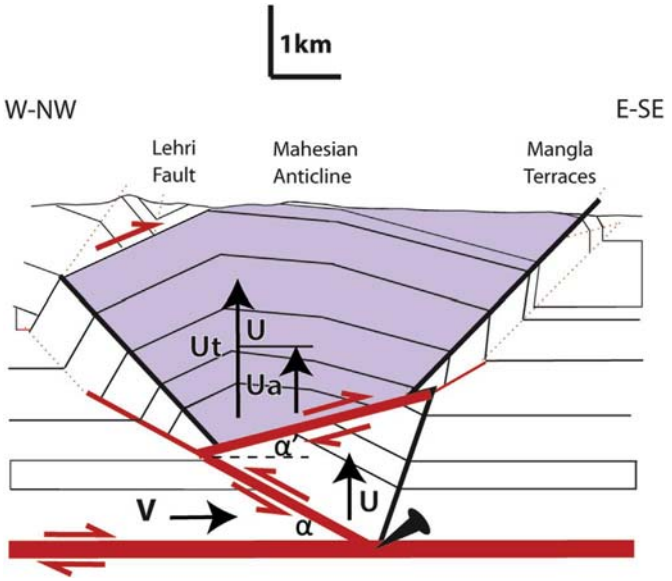

Fig. 8. a–b. Interpretation of the Holocene uplift of the Mahesian Anticline as due to a thrust and a backthurst. The violet zone is the zone located between the active axial surfaces (black lines). This is the substratum of the Mangla terraces and moves with the slip field. α and α′ are the dip angles of the thrust and backthrust, respectively. U is the uplift produced by the lower wedge, and Ua by the upper wedge. The addition of both is the total uplift Ut. V is the horizontal component of slip along the basal detachment. (For interpretation of the references to colour in this figure legend, the reader is referred to the web version of this article.)

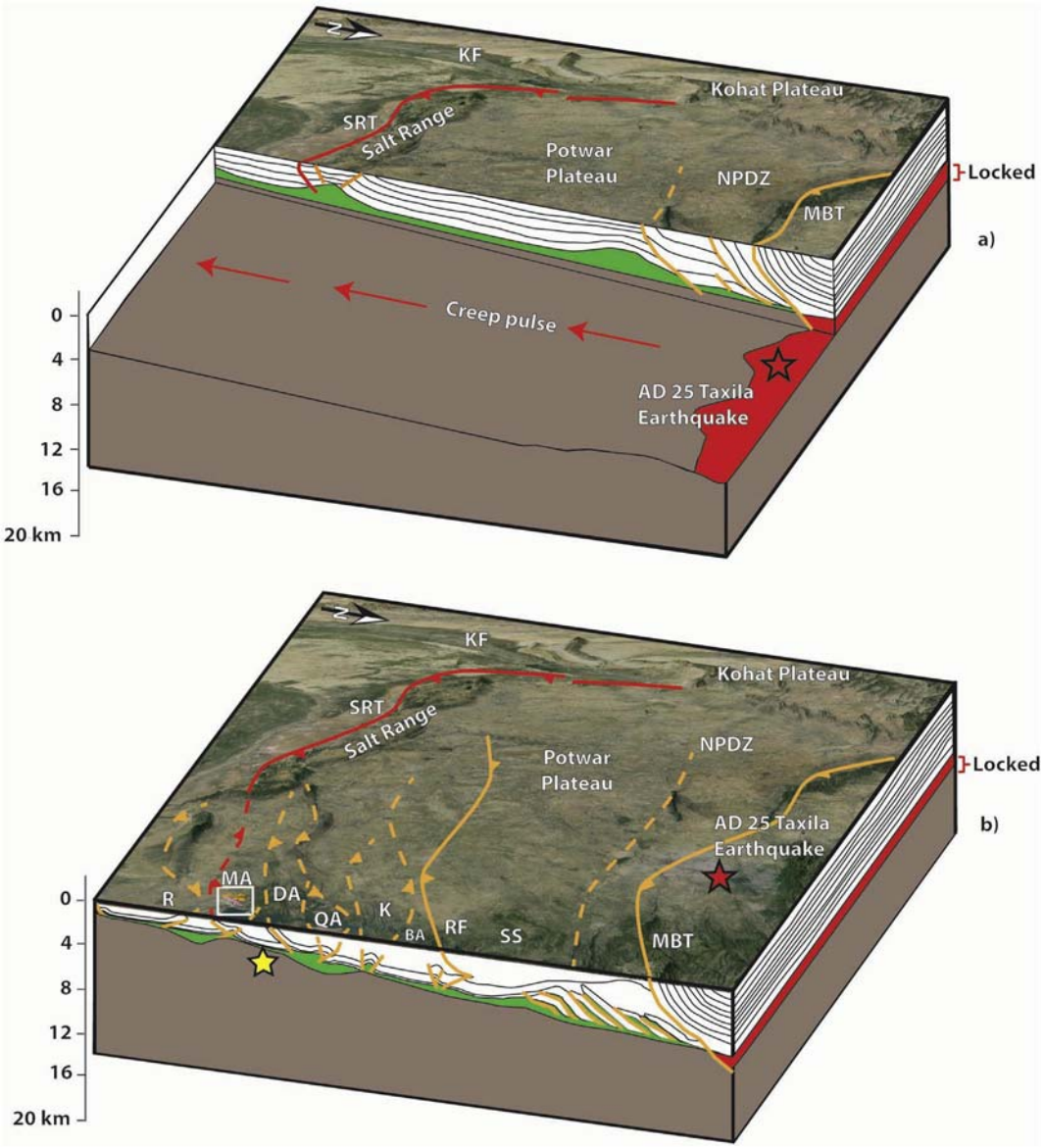

Fig. 9. a–b. Mechanisms to explain a) The hypothetical accelerated creep pulses triggered by earthquakes like the AD 25 Taxila Earthquake, and b) The hypothetical large shallow earthquakes occurring beneath the eastern Potwar Plateau. Legend is the same as for Fig. 1a and b. Yellow star in b) depicts the hypothetical shallow earthquakes beneath the Mahesian Anticline. Red and green zones represent the salt level and the locked area along the MHT, respectively. Orange lines are the thrusts in the Potwar Plateau. Red lines are the thrusts that define the more active frontal regions of this plateau. (For interpretation of the references to colour in this figure legend, the reader is referred to the web version of this article.)

MHT and/or upper thrusts in the eastern part of the Potwar Plateau are able to produce seismicity.

To estimate a maximum magnitude for an earthquake affecting the eastern part of the Potwar Plateau, we consider that the study area has not been struck by great earthquakes over the last 300 years. For a slip rate of ~10 mm/y over this period, we calculate a minimum slip deficit of 3 m. If this slip deficit were to be made up during an earthquake, the associated rupture could affect a locked zone bounded to the southwest by the portion of the MHT that currently creeps (Jouanne et al., 2014), and to the east by the Jhelum Fault, a zone where the salt thickness is usually less than 0.2 km (Leathers, 1987). This would lead to an earthquake of ~Mw 7.

If the proposed hypothesis involving great earthquakes is correct, the Holocene Mahesian Anticline development is due to successive earthquakes initiated along the MHT and that propagate along the leading thrust and/or backthrust. These ruptures would not necessarily reach the surface. Shallow depth earthquakes of ~Mw 6 have been reported beneath similar anticlines in California (Lin and Stein, 1989).

An open question is what would happen to the Mangla Dam if an earthquake struck similar to those that we interpret occurred beneath the Mahesian Anticline. With the available information and our results, we think that seismic risk associated with the occurrence of unusual large earthquakes must not be ruled out for a densely inhabited zone located in the periphery of the Mangla Dam.

9. Conclusions

- Four fluvial terraces were identified on the SE flank of the Mahesian Anticline; the maximum ages for terraces T2 and T3, dated by ^{10}Be, are 6.5 ± 0.2 ka and 3.3 ± 0.7 ka, respectively.

- Analysis of structural datasets indicates that the Mahesian Anticline has experienced a complex kinematic history since its inception. It seems to be a detachment fault truncated by a backthrust and a thrust. The propagation of the thrust induces tilting of the external limb of the fold and the uplift rate for the central part of the fold is 10.2 ± 1.5 mm/y for the Holocene.
- Shortening rates for this fold are greater than 10 mm/y for the Holocene, a value close to the 8.4 ± 0.9 mm/y shortening for the Late Cenozoic.
- During the Holocene, the Kalabagh lateral ramp, the frontal Salt Range thrust, the Mahesian structure, and the Jhelum Fault, delineate the active boundary of a single thrust sheet (the Potwar plateau) that moves above the salt level without internal deformation (without out-of-sequence thrusting).
- The small but significant difference between the Late Cenozoic deformation rates (8.4 mm/y) and the geodetic velocities (2–5 mm/y) evidenced for the central Potwar Plateau appear to be linked to episodic bursts of accelerated creeping of the thick salt level, triggered by earthquakes located to the north on the deep (>15 km) part of the MHT.
- The large difference between the Late Cenozoic deformation rates and the geodetic velocities (less than 2 mm/y) reported for the eastern Potwar Plateau is thought to be linked to the accumulation of a slip deficit around asperities formed where the salt is missing. This deficit may be made up during earthquakes potentially as great as Mw 7.

Acknowledgments

This work is part of the ANR CATTELL PAKSIS project. We are grateful to Dr. Andrew Menzies who carefully reviewed our manuscript. Joaquin Cortés-Aranda was a postdoctoral researcher on a grant from Becas Chile.

Appendix A. Supplementary data

Supplementary data related to this article can be found at http://dx.doi.org/10.1016/j.quaint.2017.02.032.

References

Ambraseys, N., Lensen, G., Moinfar, M., 1975. The Pattan Earthquake of 28 Dec., 1974. Reconnaissance Report Prepared for the Government of Pakistan and UNESCO. Paris.
Anderson, R.S., Repka, J.L., Dick, G.S., 1996. Explicit treatment of inheritance in dating depositional surfaces using in situ 10Be and 26Al. Geology 24, 47–51.
Anderson, R.V., 1927. Tertiary stratigraphy and orogeny of the northern. Punjab Geol. Soc. Am. Bull. 38, 665–720.
Avouac, J.P., 2003. Mountain building, erosion, and the seismic cycle in the Nepal Himalaya. Adv. Geophys. 46, 1–80. http://dx.doi.org/10.1016/S0065-2687(03)46001-9.
Baig, M.S., Lawrence, R.D., 1987. Precambrian to early cambrian orogenesis in the Himalaya. Kashmir. J. Geol. 5, 1–22.
Baker, D.M., Lillie, R.J., Yeats, R.S., Johnson, G.D., Yousuf, M., Zamin, A.S.H., 1988. Development of the Himalayan frontal thrust zone: salt Range, Pakistan. Geology 16, 3–7. http://dx.doi.org/10.1130/0091-7613(1988)016<0003:DOTHFT>2.3.CO;2.
Berthet, T., Ritz, J.F., Ferry, M., Pelgay, P., Cattin, R., Drukpa, D., Braucher, R., Hetényi, G., 2014. Active tectonics in eastern Himalaya: new constraints from the first morphotectonic study in southern Bhutan. Geology 42, 427–430.
Bookhagen, B., Fleitmann, D., Nishiizumi, K., Strecker, M.R., Thiede, R.C., 2006. Holocene monsoonal dynamics and fluvial terrace formation in the northwest Himalaya, India. Geology 34, 601–604. http://dx.doi.org/10.1130/G22698.1.
Bossart, P., Ottiger, R., Heller, F., 1990. Rock magnetic properties and structural development in the core of the Hazara-Kashmir Syntaxis. Tectonics 9, 103–121.
Brown, E.T., Edmond, J.M., Raisbeck, G.M., Yiou, F., Kurz, M.D., Brook, E.J., 1991. Examination of surface exposure ages of Antarctic moraines using in situ produced 10Be and 26Al. Geochim. Cosmochim. Acta 55, 2269–2283. http://dx.doi.org/10.1016/0016-7037(91)90103-C.
Butler, R.W., Coward, M.P., Harwood, G.M., Knipe, R.J., 1987. Salt control on thrust geometry, structural style and gravitational collapse along the Himalayan mountain front in the Salt Range of northern Pakistan. Dyn. Geol. Salt Relat. Struct. 399–418.
Chapple, W.M., 1978. Mechanics of thin-skinned fold-and-thrust belts. Bull. Geol. Soc. Am. 89, 1189–1198. http://dx.doi.org/10.1130/0016-7606(1978)89<1189:MOTFB>2.0.CO;2.
Chen, L., Khan, S.D., 2010. InSAR observation of the strike-slip faults in the northwest Himalayan frontal thrust system. Geosphere 6, 731–736. http://dx.doi.org/10.1130/GES00518.1.
Cotton, J.T., Koyi, H.A., 2000. Modeling of thrust fronts above ductile and frictional detachments: application to structures in the Salt Range and Potwar Plateau. Pak. Geol. Soc. Am. Bull. 112, 351–363.
Coward, M.P., Kim, J.H., 1981. Strain within thrust sheet. Geol. Soc. Lond. Spec. Publ. 9.1, 275–292.
Coward, M.P., Rex, D.C., Khan, M. a., Windley, B.F., Broughton, R.D., Luff, I.W., Petterson, M.G., Pudsey, C.J., 1986. Collision tectonics in the NW Himalayas. Geol. Soc. Lond. Spec. Publ. 19, 203–219. http://dx.doi.org/10.1144/GSL.SP.1986.019.01.11.
Crawford, A.R., 1974. The salt Range, the Kashmir syntaxis and the Pamir arc. Earth Planet. Sci. Lett. 22, 371–379.
Erslev, E.A., 1991. Trishear fault-propagation folding B. Simple Shear 617–620. http://dx.doi.org/10.1130/0091-7613(1991)019<0617.
Frankel, K.L., Owen, L.A., Dolan, J.F., Knott, J.R., Lifton, Z.M., Finkel, R.C., Wasklewicz, T., 2015. Timing and rates of Holocene normal faulting along the black mountains fault zone, death valley, USA. Lithosphere L464.1. http://dx.doi.org/10.1130/L464.1.
Gee, E.R., 1980. Salt Range Series Geological Maps, Scale 1:50 000, 6 Sheets. Directorate of Overseas Surveys, United Kingdom, for the Government of Pakistan and Pakistan Geological Survey.
Gosse, J.C., Phillips, F.M., 2001. Terrestrial in situ cosmogenic nuclides: theory and application. Quat. Sci. Rev. 20, 1475–1560. http://dx.doi.org/10.1016/S0277-3791(00)00171-2.
Grelaud, S., Sassi, W., de Lamotte, D.F., Jaswal, T., Roure, F., 2002. Kinematics of eastern salt Range and south Potwar basin (Pakistan): a new scenario. Mar. Pet. Geol. 19, 1127–1139. http://dx.doi.org/10.1016/S0264-8172(02)00121-6.
Hidy, A.J., Gosse, J.C., Pederson, J.L., Mattern, J.P., Finkel, R.C., 2010. A geologically constrained Monte Carlo approach to modeling exposure ages from profiles of cosmogenic nuclides: an example from Lees Ferry, Arizona. Geochem. Geophys. Geosyst. 11 http://dx.doi.org/10.1029/2010GC003084.
Hunsche, U., Hampel, A., 1999. Rock salt—the mechanical properties of the host rock material for a radioactive waste repository. Eng. Geol. 52, 271–291.
Jaumé, S.C., Lillie, R., 1988. Mechanics of the Salt Range-Potwar Plateau, Pakistan: a fold and thrust belt underlain by evaporates. Tectonics 7, 57–71.
Jouanne, F., Awan, A., Pêcher, A., Kausar, A., Mugnier, J.L., Khan, I., Khan, N.A., Van Melle, J., 2014. Present-day deformation of northern Pakistan from salt ranges to Karakorum ranges. J. Geophys. Res. Solid Earth 119, 2487–2503. http://dx.doi.org/10.1002/2013JB010776.Received.
Khan, I. a., Bridge, J.S., Kappelman, J., Wilson, R., 1997. Evolution of Miocene fluvial environments, eastern Potwar plateau, Northern Pakistan. Sedimentology 44, 221–251. http://dx.doi.org/10.1111/j.1365-3091.1997.tb01522.x.
Khan, S.D., Chen, L., Ahmad, S., Ahmad, I., Ali, F., 2012. Lateral structural variation along the Kalabagh Fault Zone, NW Himalayan foreland fold-and-thrust belt, Pakistan. J. Asian Earth Sci. 50, 79–87. http://dx.doi.org/10.1016/j.jseaes.2012.01.009.
Lal, D., 1991. Cosmic ray labeling of erosion surfaces: in situ nuclide production rates and erosion models: Earth and Planetary Science Letters. Earth Planet. Sci. Lett. 104, 424–439.
Lal, D., 1988. In situ-produced cosmogenic isotopes in terrestrial rocks. Annu. Rev. Earth Planet. Sci. 16, 355–388.
Leathers, M.R., 1987. Balanced Structural Cross Section of the Western Salt Range and Potwar Plateau, Pakistan: Deformation Near the Strike-slip Terminus of an Overthrust Sheet. Oregon State University.
Lillie, R.J., Johnson, G.D., Yousuf, M., Zamin, A.S.H., Yeats, R.S., 1987. Structural development within the Himalayan foreland fold-and-thrust belt of Pakistan. In: Beaumont, C., Tankard, A.J. (Eds.), Sedimentary Basins and Basin Forming Mechanisms. Mem. Can. Soc Pet. Geol., pp. 379–392.
Lin, J., Stein, R.S., 1989. Coseismic folding, earthquake recurrence, and the 1987 source mechanism at Whittier Narrows, Los Angeles basin, California. J. Geophys. Res. 94, 9614–9632.
McDougall, J.W., Hussain, A., Yeats, R.S., 1993. The Main Boundary Thrust and propagation of deformation into the foreland fold-and-thrust belt in northern Pakistan near the Indus River. Geol. Soc. Lond. Spec. Publ. 74, 581–588.
Mcdougall, J.W., Khan, S.H., 1990. Strike-slip faulting in a foreland foldthrust belt: the Kalabagh Fault and western salt Range, Pakistan. Tectonics 9, 1061–1075.
Monalisa, A.A., Qasim, A.K.M., Yeats, R.S., Hussain, A., Khan, S.H., 2009. New data on the Indus Kohistan seismic zone and its extension into the Hazara – Kashmir syntaxis, NW Himalayas of Pakistan. J. Seismol. 13, 339–361. http://dx.doi.org/10.1007/s10950-008-9117-z.
Mugnier, J.L., Becel, D., Granjeon, D., 2006. Active tectonics in the Subandean belt inferred from the morphology of the Rio Pilcomayo. In: Willett, S.D., Hovius, N., Brandon, M.T., Fisher, D. (Eds.), Tectonics, Climate and Landscape Evolution, pp. 353–369.
Mugnier, J.L., Huyghe, P., 2006. Ganges basin geometry records a pre-15 Ma isostatic rebound of Himalaya. Geology 34, 445–448. http://dx.doi.org/10.1130/G22089.1.
Mukul, M., Jaiswal, M., Singhvi, A.K., 2007. Timing of recent out-of-sequence active deformation in the frontal Himalayan wedge: insights from the Darjiling sub-

Himalaya, India. Geology 35, 999–1002. http://dx.doi.org/10.1130/G23869A.1.
Nakata, T., Tsutsumi, H., Khan, S.H., Lawrence, R.D., 1991. Active faults of Pakistan, map sheets and inventories. In: Hiroshima, vol. 21. Spec. Publ. Hiroshima Univ. Res. Cent. Reg. Geogr., Japan, p. 141.
Oskin, M., Perg, L., Shelef, E., Strane, M., Gurney, E., Singer, B., Zhang, X., 2008. Elevated shear zone loading rate during an earthquake cluster in eastern California. Geology 36, 507–510. http://dx.doi.org/10.1130/G24814A.1.
Parsons, T., Yeats, R.S., Yagi, Y., Hussain, A., 2006. Static stress change from the 8 October, 2005 M = 7.6 Kashmir earthquake. Geophys. Res. Lett. 33, 6–9. http://dx.doi.org/10.1029/2005GL025429.
Pennock, E.S., Lillie, R.J., Zaman, A.S.H., Yousuf, M., 1989. Structural interpretation of seismic reflection data from eastern Salt Range and Potwar Plateau. Pak. Am. Assoc. Pet. Geol. Bull. 73, 841–857.
Putkonen, J., Swanson, T., 2003. Accuracy of cosmogenic ages for moraines. Quat. Res. 59, 255–261. http://dx.doi.org/10.1016/S0033-5894(03)00006-1.
Rizza, M., Ritz, J.F., Prentice, C., Vassallo, R., Braucher, R., Larroque, C., Arzhannikova, A., Arzhannikov, S., Mahan, S., Massault, M., Michelot, J.L., Todbileg, M., Arnold, M., Aumaître, G., Bourlès, D., Keddadouche, K., 2015. Earthquake geology of the Bulnay fault (Mongolia). Bull. Seismol. Soc. Am. 105, 72–93. http://dx.doi.org/10.1785/0120140119.
Satyabala, S.P., Yang, Z., Bilham, R., 2012. Stick – slip advance of the Kohat Plateau in Pakistan. Nat. Geosci. 5, 147–150. http://dx.doi.org/10.1038/ngeo1373.
Schelling, D., Arita, K., 1991. Thrust tectonics, crustal shortening, and the structure of the far-eastern Nepal Himalaya. Tectonics 10, 851. http://dx.doi.org/10.1029/91TC01011.
Seeber, L., Armbruster, J.G., 1981. Great detachment earthquakes along the Himalayan Arc and long-term forecasting. In: Sibson, D.W., Richards, P.G. (Eds.), Earthquake Prediction: An international review. American Geophysical Union. Maurice Ewing Series, 4, Amer. Geophysical Union, pp. 259–277. http://dx.doi.org/10.1029/ME004p0259.
Suppe, J., 1983. Geometry and kinematics of fault-bend folding. Am. J. Sci. 283, 684–721.
Treloar, P.J., Coward, M.P., Chambers, A.F., Izatt, C.N., Jackson, K.C., 1992. Thrust geometries, interferences and rotations in the northwest Himalaya. In: McClay, K. (Ed.), Thrust Tectonics. London Chapman and Hall, London, pp. 325–342.
Trivedi, A., Chauhan, M.S., 2009. Holocene vegetation and climate fluctuations in northwest Himalaya, based on Pollen evidence from Surinsar Lake, Jammu region, India. J. Geol. Soc. India 74, 402–412.
Urai, J.L., Schléder, Z., Spiers, C.J., Kukla, P.A., 2008. Flow and transport properties of salt rocks. In: Littke, R., Bayer, U., Gajewski, D., Nelskamp, S. (Eds.), Dynamics of Complex Intracontinental Basins: the Central European Basin System. Springer-Verlag, Berlin–Heidelberg, pp. 277–290.
Vassallo, R., Mugnier, J.-L., Vignon, V., Malik, M. a., Jayangondaperumal, R., Srivastava, P., Jouanne, F., Carcaillet, J., 2015. Distribution of the late-quaternary deformation in northwestern Himalaya. Earth Planet. Sci. Lett. 411, 241–252. http://dx.doi.org/10.1016/j.epsl.2014.11.030.
Wallace, W.K., Homza, T.X., 2004. Detachment folds versus fault-propagation folds, and their truncation by thrust faults. In: McClay, K. (Ed.), Thrust Tectonics and Hydrocarbon Systems. AAPG Memoir, p. 82, 324–355.
Yeats, R., Lillie, R., 1991. Contemporary tectonics of the Himalayan frontal fault system: folds, blind thrusts and the 1905 Kangra earthquake. J. Struct. Geol. 13, 215–225.